

Size-dependent damped vibration and buckling analyses of bidirectional functionally graded solid circular nano-plate with arbitrary thickness variation

Abbas Heydari*

Young Researchers and Elite Club, Ardabil Branch, Islamic Azad University, Ardabil, Iran

(Received July 4, 2018, Revised August 11, 2018, Accepted August 17, 2018)

Abstract. For the first time, nonlocal damped vibration and buckling analyses of arbitrary tapered bidirectional functionally graded solid circular nano-plate (BDFGSCNP) are presented by employing modified spectral Ritz method. The energy method based on Love-Kirchhoff plate theory assumptions is applied to derive neutral equilibrium equation. The Eringen's nonlocal continuum theory is taken into account to capture small-scale effects. The characteristic equations and corresponding first mode shapes are calculated by using a novel modified basis in spectral Ritz method. The modified basis is in terms of orthogonal shifted Chebyshev polynomials of the first kind to avoid employing adhesive functions in the spectral Ritz method. The fast convergence and compatibility with various conditions are advantages of the modified spectral Ritz method. A more accurate multivariable function is used to model two-directional variations of elasticity modulus and mass density. The effects of nanoscale, in-plane pre-load, distributed dashpot, arbitrary tapering, pinned and clamped boundary conditions on natural frequencies and buckling loads are investigated. Observing an excellent agreement between results of current work and outcomes of previously published works in literature, indicates the results' accuracy in current work.

Keywords: non-local continuum mechanics; damped vibration; buckling; bidirectional functionally graded material; circular nano-plate; arbitrary thickness variation

1. Introduction

In contrast to the traditional composites, in the three-dimensional or bidirectional functionally graded material (BDFGM) the compositional gradients from one component to the other in two or more directions, make it possible to have a smooth and continues variations of material properties. As a result, the properties of both components can be utilized with less stress concentration and interface problem due to eliminating thermo-mechanical mismatch in components bonding. In the case of serve operating conditions like the heat-engine components, heat exchanger tubes, thermoelectric generators, rocket heat shields, plasma facings for fusion reactors and wear-resistant linings for handling large heavy abrasive ore particles, the FGM is a suitable choice. Many researchers draw attention to analyze the behavior of the structural members made up of FGM due to their benefits (Chen *et al.* 2017, Arioui *et al.* 2018, Boudherba 2018, Fallahnejad *et al.* 2018, Nejad *et al.* 2018). Also many researchers have pointed out the significance of the vibration and buckling analyses of the homogeneous and heterogeneous beams, plates and shells (Heydari and Kazemi 2009, Heydari 2011, 2013, Wang *et al.* 2014, Heydari 2015, Heydari and Kazemi 2015, Roshan and Neha 2015, Ranganathan *et al.* 2016, Heydari 2017, Lal and Ahlawat 2017, Li *et al.* 2017, Shojaeefard *et al.* 2017, Hadji

et al. 2018, Heidari *et al.* 2018, Heydari and Shariati 2018, Rossit *et al.* 2018, Sachdeva and Padhee 2018, Sun *et al.* 2018, Szymczak and Kujawa 2018, Li and Guo 2018). Also, the vibrational analysis of the plates is in focus (Ai *et al.* 2018, Gibigaye *et al.* 2018, Lei *et al.* 2018, Li *et al.* 2018, Park and Choi 2018, Shirmohammadi and Bahrami 2018, Yousefzadeh *et al.* 2018). The elastic bending behavior of a transversely isotropic FG solid circular plate subject to transverse biharmonic forces applied on its top surface is studied by virtue of the generalized England's method (Yang *et al.* 2018). Based on the three-dimensional elasticity equations, buckling analysis of symmetrical circular sandwich plates with radially graded metal foam core based on nonlinear hypothesis of deformation of the normal to the middle plane of the plate is presented (Magnucka-Blandzi *et al.* 2018). Size-dependent three-dimensional free vibration of rotating FG micro-beams based on a modified couple stress theory and von Kármán geometric nonlinearity is studied (Fang *et al.* 2018). The new approaches and techniques are the essential tools to solve new engineering problems (Toghroli *et al.* 2018). A new numerical scheme for buckling analysis of shear deformable through-thickness graded circular plate with linear and quadratic tapering patterns subjected to uniform radial compression with pinned and clamped edges rested on two-parameter elastic medium is presented (Heydari *et al.* 2017). A modified Euler-Lagrange equation is achieved and then solved by converting differential equation to an algebraic system of equations. Moreover, in mentioned work a new displacement field in polar coordinate is proposed and a novel approach for buckling analysis based on shear stress-free surface without shear correction factor

*Corresponding author, Ph.D.

E-mail: a_heydari@alum.sharif.edu or
a_heydari@tabrizu.ac.ir

requirement is carried out. The stability equation in the modified coordinate is solved by using shifted Legendre polynomials as the basis in the spectral Ritz method. The authors show that by taking small numbers of the basis, the outcomes in literature are improved. In the framework of the nonlocal strain gradient theory, the dispersion relations between phase velocity and wave number are employed to analyze wave propagation in the porous nanotubes (She *et al.* 2018). Decreasing nonlocal parameter or increasing strain gradient parameter yields to increasing of the asymptotic phase velocity. The authors show that the dispersion relations of nanotubes are affected by the material gradation and variation of the temperature, considerably. The strain gradient and nonlocal parameters have substantial effects on the dispersion relation at high wave numbers, in contrast, these effects are insignificant at low wave numbers. Moreover, they show that the power law index affects phase velocity. A refined beam model without correction factor requirement, energy variation principle and two-step perturbation method are applied for analyzing thermal buckling and post-buckling behaviors of thin radially graded hollow cylinder with pinned ends subjected to uniform temperature rise in the presence of elastic medium (She *et al.* 2018). The continuous material variation of the tube was modeled based on the conventional power law function. They report the higher buckling temperature and post-buckling strength in the case of existing an elastic foundation. The size-dependent vibration analysis of shear deformable porous nanotubes with radial gradation of the temperature-dependent material based on refined beam model in the framework of the nonlocal strain gradient theory is conducted by employing Navier solution method (She *et al.* 2018). The thermal buckling and post-buckling behavior of the nonlocal tubes made up of temperature-dependent radially functionally graded materials with the both even and uneven porosity distributions is performed by applying a refined shear deformation beam theory in the framework of the Eringen nonlocal continuum mechanics (She *et al.* 2017). The stability equations are derived by using the generalized variation principle and solved via two-step perturbation method. The authors show that the small-scale parameter and porosity volume fraction change the buckling and post-buckling behavior of the nanotubes. The nonlinear bending, thermal buckling and post-buckling analyses of shear deformable temperature-dependent radially graded material tubes with two clamped ends are investigated by satisfying the traction-free natural conditions on the inner and outer surfaces without shear correction factor requirement (She *et al.* 2017). In the mentioned research, a two-step perturbation method is applied to obtain the asymptotic solutions of the FGM tubes under nonlinear bending and thermal post-buckling. The nonlinear bending behaviors of the infinite temperature-dependent radially graded material cylindrical shallow shells with pinned or clamped ends subjected to the uniform temperature rise rested on two-parameter elastic medium is predicted by employing two-step perturbation method (She *et al.* 2017). In this research, the authors claim that FGM cylindrical shallow shells subjected to uniform bending loadings will bring about

snap-through buckling and jump changes, but the foundation can increase the stability of the shells. The thermal buckling loads and post-buckling equilibrium paths of FG beams with clamped boundary conditions subjected to uniform temperature rise are calculated based on various beam models including Euler-Bernoulli, Timoshenko and various higher-order shear deformation beam theories via two-step perturbation method (She *et al.* 2017). The governing equations are developed with respect to the neutral plane and temperature dependency of the constituents. In the mentioned research, it is shown that in the case of uniform temperature rise loading, the post-buckling equilibrium path is also of the bifurcation type for any arbitrary value of the power law index and various displacement fields. The thermal buckling loads and post-buckling equilibrium paths of temperature-dependent transversely material graded beams with surface-bonded piezoelectric actuators exposed to uniform temperature and electric fields are calculated based on high-order shear deformation theory, physical neutral surface concept and nonlinear von Kármán strain-displacement relationship (She *et al.* 2017). Mechanical buckling of FG polyethylene/clay nanocomposites columns based on the Engesser-Timoshenko beam theory is performed (Yas and Khorramabadi 2018).

For the first time, damped vibration and buckling analyses of love-Kirchhoff arbitrary tapered bidirectional functionally graded solid circular nano-plate (BDFGSCNP) resting on viscous medium with pinned and clamped boundary conditions at edge of the plate is presented. At present, notable developments in modeling and simulation of functionally graded materials (FGMs) have been reported (Gupta and Talha 2015). In light of these efforts on FGMs, it is possible to tailor material composition so as to get maximum aids from their inhomogeneity. In current work, a four variable function is used to model two-directional variations of elasticity modulus and mass density based on classical rule of mixture. However, in contrast to the conventional exponential gradation, the analysis of BDFGSCNP based on this function needs more computational efforts, but the more accurate variations of mechanical and material properties can be modeled. The energy method is employed to derive neutral equilibrium equation then the characteristic equations are calculated via modified spectral Ritz method. In present paper, the orthogonal shifted Chebyshev polynomials of the first kind in modified coordinate is proposed as the basis in spectral Ritz method. The novel proposed basis not only satisfies boundary conditions, but also removes the difficulties of calculating appropriate auxiliary functions in spectral Ritz method. However, the proposed modified basis is used for vibration and buckling analyses of BDFGSCNP, but it can be used for other analyses like the bending and post-buckling problems of nanoscale and macroscale BDFGCPs. Observing an excellent agreement between results of the current work and outcomes of the previously published works in literature, indicates the accuracy of the calculated results in current work.

2. Neutral equilibrium equation

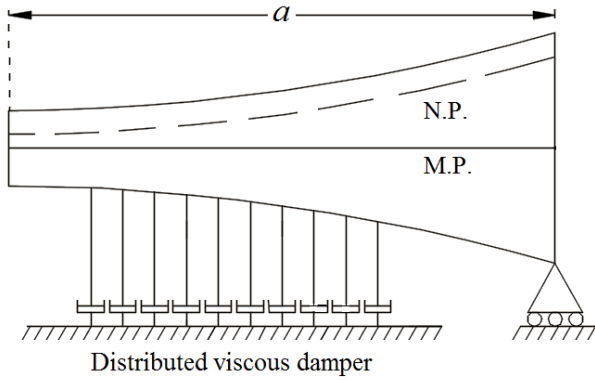


Fig. 1 The tapered BDFGSCNP rested on distributed viscous damper

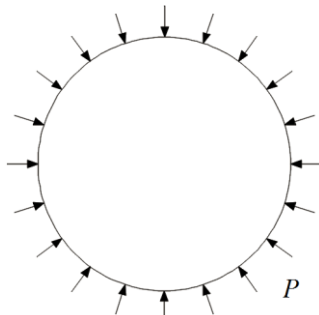


Fig. 2 The uniform mechanical loading at edge of the plate

The geometrical properties and uniform mechanical loading of pinned BDFGSCNP with nonlinear thickness variation and positive taper constant rested on the distributed viscous damper are shown in Figs. 1 and 2, respectively. The mid-plane and neutral plane are shown by M.P. and N.P., respectively.

It is assumed that the variations of mass density and elasticity modulus are product of two separable functions in terms of z and r in cylindrical coordinate. The functions of elasticity modulus variations for transverse and radial directions are denoted by E_z (or $E_{\bar{z}}$ in neutral plane coordinate) and E_r , respectively ($E = E_z E_r$). Similarly, the mass density variations in bending and radial directions are denoted by ρ_z and ρ_r , respectively ($\rho = \rho_z \rho_r$). The mass density and elasticity modulus are defined based on four parameters and two material indexes as follows

$$\rho(r, z) = \left((\rho_t - \rho_b) \left(\frac{z}{t} + \frac{1}{2} \right)^{n_t} + \rho_b \right) \left((\rho_a - \rho_0) \left(\frac{r}{a} \right)^{n_r} + \rho_0 \right) \quad (1)$$

$$E(r, z) = \left((E_t - E_b) \left(\frac{z}{t} + \frac{1}{2} \right)^{n_t} + E_b \right) \left((E_a - E_0) \left(\frac{r}{a} \right)^{n_r} + E_0 \right)$$

In Eq. (1), the non-negative parameters n_t and n_r are material constants or material indexes in transverse and radial directions, respectively. For the case $\rho_0 = \rho_a = E_0 = E_a = 1$, $E_t = E_c$, $E_b = E_m$, $\rho_t = \rho_c$, and $\rho_b = \rho_m$

the plate has transverse gradient and top and bottom surfaces are pure ceramic and pure metal, respectively. The parameters E_m , E_c , ρ_m and ρ_c are elasticity modulus and mass density of metal and ceramic. Similarly, for the case $\rho_b = \rho_t = E_b = E_t = 1$, $E_0 = E_m$, $E_a = E_c$, $\rho_0 = \rho_m$, and $\rho_a = \rho_c$ the plate has radial gradient and center and edge of the plate are pure metal and pure ceramic, respectively. Also, for the cases ($n_r = 0$) or ($n_t = 0$), radial or transverse gradations are vanished, respectively. For other cases, the plate is turned to BDFGCP. It is noteworthy to mention that in the case of radial gradation the four coefficients E_b , E_t , ρ_b and ρ_t are dimensionless. Also, in the case of transverse gradation the four coefficients E_0 , E_a , ρ_0 and ρ_a are dimensionless. The bending strain energy of bidirectional functionally graded solid circular plate (BDFGSCP) by considering axisymmetric condition is calculated based on assumptions of Love-Kirchhoff plate theory after neglecting transverse shear displacement effects as follows

$$U_{\text{Plate}} = \frac{\pi}{1 - \nu^2} \int_0^a \int_{-\frac{t}{2}}^{\frac{t}{2}} (\epsilon_r^2 + \epsilon_\theta^2 + 2\nu\epsilon_r\epsilon_\theta) E dz r dr \quad (2)$$

In Eq. (2), the parameters ϵ_r and ϵ_θ are radial strain and circumferential strain, respectively. The poisson's ratio, ν , is assumed to be constant. The arbitrary thickness variation of the plate is assumed as follows

$$t = t_0 \left(1 + \alpha \left(\frac{r}{a} \right)^\beta \right) \quad (3)$$

In Eq. (3), the parameter α is taper constant which takes real values. For $\beta = 1$ the thickness variation is linear and for $\beta > 1$, it is nonlinear. For plate with uniform thickness α (or β) is zero. Thickness at center of the BDFGSCP is presented by the parameter t_0 . The distance between N.P. and M.P., z_0 , is calculated as follows

$$z_0 = \frac{t_0 n_t (E_t - E_b)}{2(n + 2)(n E_b + E_t)} \left(1 + \alpha \left(\frac{r}{a} \right)^\beta \right) \quad (4)$$

After transforming coordinate from M.P. to N.P., Eq. (2) can be rewritten as follows

$$\pi \int_0^a D E_r \left((w^{(2)})^2 + \left(\frac{w^{(1)}}{r} \right)^2 + \frac{2\nu w^{(1)} w^{(2)}}{r} \right) r dr \quad (5)$$

The symbol w denotes the transverse displacement or deflection of the BDFGCP. The j^{th} derivative of w with respect to r is presented by $w^{(j)}$. The bending rigidity of the FGSCP, D , is calculated for $n_t \geq 0$, as follows

$$D = \frac{t_0^3}{12(1 - \nu^2)} \left(1 + \alpha \left(\frac{r}{a} \right)^\beta \right) \times \frac{\psi_1 E_b^2 + \psi_2 E_b E_t + 12 E_t^2}{\psi_3 E_b + \psi_4 E_t + 12 E_t} \quad (6)$$

The constants ψ_1 to ψ_4 are

$$\begin{aligned} \psi_1 &= n_t^4 + 4n_t^3 + 7n_t^2 \\ \psi_2 &= 4n_t^3 + 16n_t^2 + 28n_t \\ \psi_3 &= n_t^4 + 7n_t^3 + 16n_t^2 + 12n_t \\ \psi_4 &= n_t^3 + 7n_t^2 + 16n_t \end{aligned} \tag{7}$$

The response of the viscous medium is

$$f_{\text{damper}} = C_d \frac{\partial w}{\partial t} \tag{8}$$

where the parameter t denotes time. The Eringen's nonlocal continuum theory is based on continuum mechanics approach, in which the stress tensor at a point depends on strain tensor at all points in domain of the material. Based on Eringen's nonlocal continuum theory the relation between nonlocal stress, σ^{NL} , and local stress, σ^L , can be expressed as $(1 - \eta^2 \nabla^2) \sigma^{NL} = \sigma^L$, in which η is scale coefficient. The energy of nonconservative forces, after using relation between nonlocal stress and local stress is calculated as follows

$$\Omega_{\text{damper}} = \pi I \int_0^a c_d \omega \left(w^2 - \eta^2 w \left(w^{(2)} + \frac{w^{(1)}}{r} \right) \right) r dr \tag{9}$$

in which I is one of the square roots of -1. The kinematic energy caused by vibration is calculated as follows

$$U_\omega = - \frac{\pi \omega^2 t_0 (n_t \rho_b + \rho_t)}{n_t + 1} \int_0^a \rho_r \left(1 + \alpha \left(\frac{r}{a} \right)^\beta \right) \left(w^2 + \eta^2 (w^{(1)})^2 \right) r dr \tag{10}$$

The Eq. (10) is precise for constant amounts or little changes of ρ_r and t . The work done by uniform radial compression at edge of the BDFGSCNP is as follows

$$\Omega = -\pi P \int_0^a \left((w^{(1)})^2 + \eta^2 \left(\left(\frac{w^{(1)}}{r} \right)^2 + (w^{(2)})^2 \right) \right) r dr \tag{11}$$

The sign of P for compression is taken to be positive. The neutral equilibrium equation is computed by setting total potential energy equal to zero as follows

$$\begin{aligned} & \int_0^a \left[\frac{c_1 E_b^2 + c_2 E_b E_t + 12 E_t^2}{c_3 E_b + c_4 E_t + 12 E_t} \frac{t_0^3}{12(1 - \nu^2)} \right. \\ & \left. \left((E_a - E_0) \left(\frac{r}{a} \right)^{n_r} + E_0 \right) \left(1 + \alpha \left(\frac{r}{a} \right)^\beta \right) \right. \\ & \left. \left((w^{(2)})^2 + \left(\frac{w^{(1)}}{r} \right)^2 + \frac{2\nu w^{(1)} w^{(2)}}{r} \right) + \right. \\ & \left. c_d I \omega w^2 - \frac{\omega^2 t_0 (n_t \rho_b + \rho_t)}{n + 1} \left(1 + \alpha \left(\frac{r}{a} \right)^\beta \right) \right. \\ & \left. \left((\rho_a - \rho_0) \left(\frac{r}{a} \right)^{n_r} + \rho_0 \right) w^2 - P (w^{(1)})^2 - \right. \end{aligned} \tag{12}$$

$$\eta^2 \left[P \left(\left(\frac{w^{(1)}}{r} \right)^2 + (w^{(2)})^2 \right) + c_d I \omega w \right.$$

$$\left. \left(w^{(2)} + \frac{w^{(1)}}{r} \right) + \frac{\omega^2 t_0 (n_t \rho_b + \rho_t)}{n_t + 1} \left(1 + \alpha \left(\frac{r}{a} \right)^\beta \right) \right. \\ \left. (w^{(1)})^2 \left((\rho_a - \rho_0) \left(\frac{r}{a} \right)^{n_r} + \rho_0 \right) \right] r dr = 0$$

3. Vibration and buckling analysis

In current research, the spectral Ritz method with a modified basis in terms of orthogonal shifted Chebyshev polynomials of the first kind is proposed to calculate optimum deflection and corresponding damped frequencies and buckling loads of first modes. The Chebyshev polynomial of order n is presented by $C_n(r)$. The Chebyshev polynomials of the first kind are orthogonal in the interval $[-1,1]$ with respect to the weight function $1/\sqrt{1 - r^2}$.

$$C_n(r) = \cos(n \times \text{Arccos}(r)) \tag{13}$$

Eq. (14) presents approximated bending displacement function. The function w in polar coordinate is replaced by the function \bar{w} in modified coordinate $\bar{r} = 2(r/a) - 1$, in which $\bar{w}(\bar{r}) = w((1 + \bar{r}) a/2)$.

$$\bar{w}(\bar{r}) \approx \gamma_m^T \Gamma_m, \quad -1 \leq \bar{r} \leq 1 \tag{14}$$

In Eq. (14), Γ_m and γ_m are basis vector and coefficient vector with $m + 1$ rows, respectively.

$$\Gamma_m = \begin{Bmatrix} C_0(\bar{r}) \\ C_1(\bar{r}) \\ C_2(\bar{r}) \\ \vdots \\ C_m(\bar{r}) \end{Bmatrix}, \quad \gamma_m = \begin{Bmatrix} \lambda_0 \\ \lambda_1 \\ \lambda_2 \\ \vdots \\ \lambda_m \end{Bmatrix} \tag{15}$$

The orthogonality of $C_n(\bar{r})$ in the interval $[-1,1]$ with respect to the weight function $1/\sqrt{1 - \bar{r}^2}$ is shown as follows

$$\int_{-1}^1 \frac{C_p(\bar{r}) C_q(\bar{r})}{\sqrt{1 - \bar{r}^2}} d\bar{r} = \begin{cases} 0 & p \neq q \\ \pi & p = q = 0 \\ \pi/2 & p = q \neq 0 \end{cases} \tag{16}$$

After satisfying boundary conditions, the coefficients λ_0 to λ_{c-1} in the coefficient vector will be calculated in terms of the coefficients λ_c to λ_m . The number of boundary equations are equal to c . In the case of FGSCP, the parameter c is equal to 3. In current work, boundary conditions are $\bar{w}(1) = \bar{w}^{(1)}(-1) = 0$. After satisfying boundary equations the coefficients λ_0 and λ_1 are calculated in terms of the remaining coefficients in γ_m vector.

$$\lambda_0 = \begin{Bmatrix} -5 \\ 8 \\ -17 \\ \vdots \\ (-1)^{m+1} m^2 - 1 \end{Bmatrix}^T \begin{Bmatrix} \lambda_2 \\ \lambda_3 \\ \lambda_4 \\ \vdots \\ \lambda_m \end{Bmatrix}, \tag{17}$$

$$\lambda_1 = \begin{Bmatrix} 4 \\ -9 \\ 16 \\ \vdots \\ (-1)^m m^2 \end{Bmatrix}^T \begin{Bmatrix} \lambda_2 \\ \lambda_3 \\ \lambda_4 \\ \vdots \\ \lambda_m \end{Bmatrix}$$

Thereafter, the coefficients λ_0 to λ_{c-1} are obtained in terms of the coefficients λ_c to λ_m by satisfying boundary condition at edge of the plate. For this purpose, the first and second derivatives of $C_n(\bar{r})$ with respect to \bar{r} are calculated as follows

$$\begin{aligned} C_n^{(1)}(\bar{r}) &= \frac{n(C_n(\bar{r})\bar{r} - C_{n-1}(\bar{r}))}{\bar{r}^2 - 1}, \\ C_n^{(2)}(\bar{r}) &= \frac{n}{(\bar{r}^2 - 1)^2} [(n - 1)C_{n-2}(\bar{r}) \\ &\quad + (3 - 2n)\bar{r}C_{n-1}(\bar{r}) \\ &\quad + ((n - 1)\bar{r}^2 - 1)C_n(\bar{r})] \end{aligned} \quad (18)$$

Eqs. (18) are used to write boundary condition of clamped edge in modified coordinate, \bar{r} , as follows

$$\sum_{n=1}^m n^2 \lambda_n = 0 \quad (19)$$

In the case of clamped edge, considering Eqs. (17) and Eq. (19), one has

$$\begin{aligned} \lambda_0 &= \begin{Bmatrix} 8 \\ 3 \\ 24 \\ \vdots \\ \frac{m^2}{8}(5 + 3(-1)^{m+1}) - 1 \end{Bmatrix}^T \begin{Bmatrix} \lambda_3 \\ \lambda_4 \\ \lambda_5 \\ \vdots \\ \lambda_m \end{Bmatrix}, \\ \lambda_1 &= \begin{Bmatrix} -9 \\ 0 \\ -25 \\ \vdots \\ \frac{m^2}{2}((-1)^m - 1) \end{Bmatrix}^T \begin{Bmatrix} \lambda_3 \\ \lambda_4 \\ \lambda_5 \\ \vdots \\ \lambda_m \end{Bmatrix}, \\ \lambda_2 &= \begin{Bmatrix} 0 \\ -4 \\ 0 \\ \vdots \\ -\frac{m^2}{8}((-1)^m + 1) \end{Bmatrix}^T \begin{Bmatrix} \lambda_3 \\ \lambda_4 \\ \lambda_5 \\ \vdots \\ \lambda_m \end{Bmatrix}. \end{aligned} \quad (20)$$

Eqs. (18) are used to write boundary condition of pinned edge in modified coordinate, \bar{r} , as follows

$$\sum_{n=1}^m (3vn^2 + 2(n^4 - n^2)) \lambda_n = 0 \quad (21)$$

In the case of pinned edge, considering Eqs. (17) and Eq. (21), one has

$$\lambda_0 = \begin{Bmatrix} 5(9\zeta - \varsigma_3)/\varrho + 8 \\ -5(16\zeta + \varsigma_4)/\varrho - 17 \\ 5(25\zeta - \varsigma_5)/\varrho + 24 \\ \vdots \\ \Lambda_m^0 \end{Bmatrix}^T \begin{Bmatrix} \lambda_3 \\ \lambda_4 \\ \lambda_5 \\ \vdots \\ \lambda_m \end{Bmatrix}, \quad (22)$$

$$\begin{aligned} \lambda_1 &= \begin{Bmatrix} 4(-9\zeta + \varsigma_3)/\varrho - 9 \\ 4(16\zeta + \varsigma_4)/\varrho + 16 \\ 4(-25\zeta + \varsigma_5)/\varrho - 25 \\ \vdots \\ \Lambda_m^1 \end{Bmatrix}^T \begin{Bmatrix} \lambda_3 \\ \lambda_4 \\ \lambda_5 \\ \vdots \\ \lambda_m \end{Bmatrix}, \\ \lambda_2 &= \begin{Bmatrix} (-9\zeta + \varsigma_3)/\varrho \\ (16\zeta + \varsigma_4)/\varrho \\ (-25\zeta + \varsigma_5)/\varrho \\ \vdots \\ \Lambda_m^2 \end{Bmatrix}^T \begin{Bmatrix} \lambda_3 \\ \lambda_4 \\ \lambda_5 \\ \vdots \\ \lambda_m \end{Bmatrix}. \end{aligned}$$

The unknown parameters in Eqs. (22) are presented in Eqs. (23).

$$\begin{aligned} \zeta &= -3\nu, \\ \varrho &= 24(1 + \nu), \\ \varsigma_m &= (2 - 3\nu)m^2 - 2m^4, \\ \Lambda_m^0 &= -5((-1)^m m^2 \zeta + \varsigma_m)/\varrho + (-1)^{m+1} m^2 - 1, \\ \Lambda_m^1 &= 4((-1)^m m^2 \zeta + \varsigma_m)/\varrho + (-1)^m m^2, \\ \Lambda_m^2 &= ((-1)^m m^2 \zeta + \varsigma_m)/\varrho \end{aligned} \quad (23)$$

The Eq. (14) is rewritten as follows

$$\bar{w}(\bar{r}) \approx \bar{\gamma}_m^T \bar{F}_m, \quad -1 \leq \bar{r} \leq 1 \quad (24)$$

in which, \bar{F}_m is modified basis vector for clamped or pinned edge and $\bar{\gamma}_m$ is coefficient vector with $m - c + 1$ rows. In the case of clamped edge, one has

$$\begin{aligned} \bar{F}_m &= \begin{Bmatrix} 8 - 9\bar{r} + C_3(\bar{r}) \\ 3 - 4(2\bar{r}^2 - 1) + C_4(\bar{r}) \\ 24 - 25\bar{r} + C_5(\bar{r}) \\ \vdots \\ \frac{m^2}{8}(\delta_0 + \bar{r}\delta_1 + (1 - 2\bar{r}^2)\delta_2) - 1 + C_m(\bar{r}) \end{Bmatrix}^T, \\ \bar{\gamma}_m &= \begin{Bmatrix} \lambda_3 \\ \lambda_4 \\ \lambda_5 \\ \vdots \\ \lambda_m \end{Bmatrix} \end{aligned} \quad (25)$$

where the parameters δ_0 to δ_2 are

$$\begin{aligned} \delta_0 &= \begin{cases} 2 & m \in \text{Even} \\ 8 & m \in \text{Odd} \end{cases} \\ \delta_1 &= \begin{cases} 0 & m \in \text{Even} \\ -8 & m \in \text{Odd} \end{cases} \end{aligned} \quad (26)$$

$$\delta_2 = \begin{cases} 2 & m \in \text{Even} \\ 0 & m \in \text{Odd} \end{cases}$$

In the case of pinned edge, it holds

$$\bar{F}_m = \begin{Bmatrix} \Lambda_3^0 + \bar{r}\Lambda_3^1 + (2\bar{r}^2 - 1)\Lambda_3^2 + C_3(\bar{r}) \\ \Lambda_4^0 + \bar{r}\Lambda_4^1 + (2\bar{r}^2 - 1)\Lambda_4^2 + C_4(\bar{r}) \\ \Lambda_5^0 + \bar{r}\Lambda_5^1 + (2\bar{r}^2 - 1)\Lambda_5^2 + C_5(\bar{r}) \\ \vdots \\ \Lambda_m^0 + \bar{r}\Lambda_m^1 + (2\bar{r}^2 - 1)\Lambda_m^2 + C_m(\bar{r}) \end{Bmatrix}^T, \quad (27)$$

$$\bar{\gamma}_m = \begin{Bmatrix} \lambda_3 \\ \lambda_4 \\ \lambda_5 \\ \vdots \\ \lambda_m \end{Bmatrix}$$

The neutral equilibrium equation is rewritten in modified coordinate, \bar{r} , as follows

$$\int_0^a \left[\frac{c_1 E_b^2 + c_2 E_b E_t + 12 E_t^2}{c_3 E_b + c_4 E_t + 12 E_t} \frac{4 t_0^3}{3(1 - \nu^2)} \right. \\ \left. \left((E_a - E_0) \left(\frac{1 + \bar{r}}{2} \right)^{n_r} + E_0 \right) \left(1 + \alpha \left(\frac{1 + \bar{r}}{2} \right) \right)^{3\beta} \right. \\ \left. \left((\bar{w}^{(2)})^2 + \left(\frac{\bar{w}^{(1)}}{1 + \bar{r}} \right)^2 + \frac{2\nu \bar{w}^{(1)} \bar{w}^{(2)}}{1 + \bar{r}} \right) + a^4 c_d I \omega \bar{w}^2 \right. \\ \left. - \frac{\omega^2 a^4 t_0 (n_t \rho_b + \rho_t)}{n + 1} \left(1 + \alpha \left(\frac{1 + \bar{r}}{2} \right) \right)^\beta \right. \\ \left. \left((\rho_a - \rho_0) \left(\frac{1 + \bar{r}}{2} \right)^{n_r} + \rho_0 \right) \bar{w}^2 - 4 P a^2 (\bar{w}^{(1)})^2 - \right. \\ \left. \eta^2 [16 P \left(\left(\frac{\bar{w}^{(1)}}{1 + \bar{r}} \right)^2 + (\bar{w}^{(2)})^2 \right) + 4 a^2 c_d I \omega \right. \\ \left. \left(\bar{w}^{(2)} + \frac{\bar{w}^{(1)}}{1 + \bar{r}} \right) \bar{w} + \frac{2 a \omega^2 t_0 (n_t \rho_b + \rho_t)}{n_t + 1} (\bar{w}^{(1)})^2 \right. \\ \left. \left. \left(1 + \alpha \left(\frac{1 + \bar{r}}{2} \right) \right)^\beta \left((\rho_a - \rho_0) \left(\frac{1 + \bar{r}}{2} \right)^{n_r} + \rho_0 \right) \right] \right] \quad (28)$$

The unknown coefficients λ_c to λ_m are determined to calculate optimum deflection function in Eq. (24) and minimum amount of P or ω in Eq. (28). For this purpose, following equations must be satisfied

$$\frac{\partial \Pi}{\partial \lambda_i} = 0, \quad i \in \{c, c + 1, c + 2, \dots, m\} \quad (29)$$

The characteristic equation of tapered BDFGSCNP is calculated by vanishing determinant of coefficient matrix of homogeneous equations in Eq. (29). The M^{th} positive root of the characteristic equation is damped natural frequency or buckling load of M^{th} mode. The buckling deflection or mode shape of transverse oscillating nonlocal tapered BDFGSCP for M^{th} mode with clamped or pinned support at edge of the plate in the presence of viscous medium is obtained by calculating coefficient vector as follows

$$\bar{\gamma}_m = \begin{Bmatrix} -[Y_1]_{(m-c) \times (m-c)}^{-1} \{Y_2\}_{(m-c) \times 1} \\ 1 \end{Bmatrix} \lambda_m \quad (30)$$

The element located in i^{th} row and j^{th} column of coefficient matrix, Y , is the coefficient of the λ_{j+c-1} in derivative of Π with respect to λ_{i+c-1} ($i, j \in \{1, 2, 3, \dots, m - c + 1\}$). The matrix $[Y_1]$ is constructed by deleting last row and last column of matrix $[Y]$. The column vector $\{Y_2\}$ is the last column of matrix Y , in which the last row is deleted. It is noteworthy to mention that for buckling or vibration analysis, the vector $\{Y_2\}$ and inverse of the matrix $[Y_1]$ are calculated by assuming P or ω equal to M^{th} positive root of the characteristic equation, respectively.

4. Numerical results

For conducting numerical analyses, the numerical values of geometrical properties, mechanical properties and dimensionless parameters are assumed as follows.

Table 1 The numerical values of geometrical properties of macroscale plate

a (m)	t_0 (m)
0.5	0.02

Table 2 The numerical values of mechanical properties

E_0 (GPa)	E_a (GPa)	ρ_0 ($\frac{\text{kg}}{\text{m}^3}$)	ρ_a ($\frac{\text{kg}}{\text{m}^3}$)	c_d ($\frac{\text{MN.s}}{\text{m}^3}$)
70	380	2700	3970	0.01

Table 3 The numerical values of dimensionless parameters

n_r	n_t	ν	α	β
1	1	0.3	0.1	1

The ratio of E_t/E_b for buckling analysis and the ratios of E_t/E_b and ρ_t/ρ_b for vibration analysis are assumed equal to R . For the case that the viscous medium is neglected, the dimensionless buckling load of BDFGSCP ($P a^2/D_0$) is independent from dimensionless parameter R , but the dimensionless undamped natural frequency of BDFGSCP ($\omega a^2 \sqrt{\rho_0 t_0/D_0}$) is dependent on R . Since the parameter R does not affect radial gradation, which is the main part of this study, this parameter can be taken equal to 1. In the case of $R = 1$, the BDFGSCP is turned to radially functionally graded solid circular plate (RFGSCP). As an example, the effect of parameter R on frequencies is presented in numerical results section. The subscript zero in dimensionless buckling load and normalized damped angular frequency of vibration denotes the value of the quantities at center of the plate ($D_0 = E_0 D$). For numerical examples, the numerical values in Table (1) to Table (3) are used unless certain numerical values were mentioned. The comparison and validity of the results, buckling and vibration results for local plate as well as results for size-dependent analysis are presented in numerical result section. Fig. 3(a) illustrates error plot as well as convergence of modified spectral Ritz method for nonlocal critical load of clamped BDFGSCNP and Fig. 3(b) illustrates error plot as well as convergence of modified spectral Ritz method for nonlocal damped angular frequency of vibration for third mode (without in-plane pre-load). It is noteworthy to mention that for small number of basis vector components, the relative error of fundamental and second frequencies are approached to zero. Increasing number of rows in basis vector yields to decreasing error percent. The subscript m in P_m or ω_m denotes value of nonlocal first buckling load or nonlocal third damped natural frequency corresponding to basis vector with m rows ($\eta/a = 0.1$). According to Fig. 3, using basis vector with small dimension, yields to obtain results with high

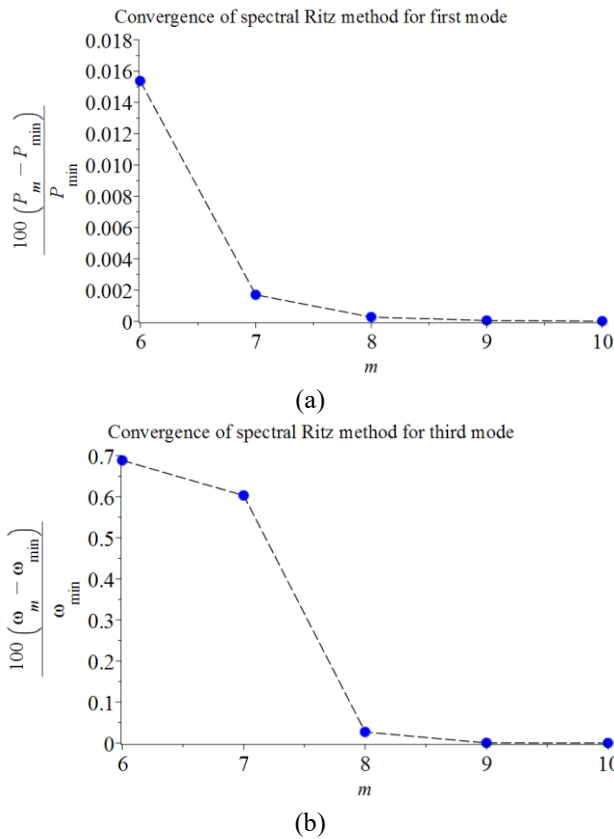


Fig. 3 The convergence of spectral Ritz method for (a) buckling and (b) vibration analysis

accuracy. Fig. 3 shows that the convergence for vibrational analysis is more than buckling analysis.

The results of current work are compared and validated with the known data in literature. Buckling analysis results of local transverse functionally graded solid circular plate (FGSCP), ($\eta = 0$, $E_0 = E_a = 1$), with linear thickness variation ($\beta = 1$) are compared with previously published results in literature (Nae *et al.* 2007). The results show an excellent agreement for various values of Poisson’s ratio (ν), taper constant (α) and various boundary conditions of FGSCP. It is noteworthy to mention that the results are independent from R . Increasing Poisson’s ratio yields to increasing critical load of clamped FGSCP with negative taper constant and yields to decreasing critical load of clamped FGSCP with positive taper constant. The critical load of uniform thin FGSCP ($\beta = 0$) with clamped edge is independent from Poisson’s ratio. The critical load of simply supported FGSCP increased by increasing Poisson’s ratio. Increasing taper constant, yields to increasing critical load of simply supported and clamped FGSCPs.

The results of current work for undamped free vibration analysis are compared with the available results in literature (Liew *et al.* 2006, Mohammadi *et al.* 2013, Mohammadi *et al.* 2013). However different geometrical and mechanical properties are used in various references, but the same results are obtained due to independency of normalized frequency from mentioned properties. The results in Tables 5 and 6 are calculated for circular plate of diameter d by setting the parameters n_r , n_t , c_d and α equal to zero.

Table 4 Result validation for buckling analysis (Pa^2/D_0)

Boundary condition	ν	α				
		0.3	-0.1	0.0	0.1	0.3
Pinned-Naei <i>et al.</i> (Naei <i>et al.</i> 2007)	0.0	1.916	2.857	3.389	3.985	5.380
	0.1	2.144	3.103	3.668	4.296	5.758
	0.2	2.325	3.343	3.937	4.594	6.110
	0.3	2.503	3.577	4.199	4.879	6.438
	0.4	2.680	3.805	4.448	5.150	6.741
Pinned-Present work	0.0	1.9616	2.8571	3.3899	3.9852	5.3804
	0.1	2.1444	3.1033	3.6687	4.2969	5.7584
	0.2	2.3251	3.3433	3.9379	4.5947	6.1107
	0.3	2.5036	3.5772	4.1977	4.8791	6.4381
	0.4	2.6802	3.8052	4.4487	5.1505	6.7416
Clamped-Naei <i>et al.</i> (Naei <i>et al.</i> 2007)	0.0	7.706	12.081	14.681	17.566	24.213
	0.1	7.822	12.135	14.681	17.496	23.952
	0.2	7.938	12.188	14.681	17.427	23.691
	0.3	8.054	12.242	14.681	17.357	23.429
	0.4	8.169	12.296	14.681	17.287	23.167
Clamped-Present work	0.0	7.7061	12.0815	14.6819	17.5666	24.2135
	0.1	7.8224	12.1352	14.6819	17.4968	23.9525
	0.2	7.9383	12.1889	14.6819	17.4269	23.6911
	0.3	8.0540	12.2425	14.6819	17.3570	23.4294
	0.4	8.1693	12.2961	14.6819	17.2871	23.1674

Table 5 Result validation for vibration of simply supported circular nano-plate ($\omega\sqrt{\rho t d^4/\pi^4 D}$)

Results	η/a										
	0.00	0.02	0.04	0.06	0.08	0.10	0.12	0.14	0.16	0.18	0.20
(Liew <i>et al.</i> 2006)	2.000	1.997	1.990	1.974	1.964	1.944	1.921	1.895	1.866	1.835	1.802
(Mohammadi <i>et al.</i> 2013)	2.000	1.997	1.990	1.974	1.964	1.944	1.921	1.895	1.866	1.835	1.802
(Mohammadi <i>et al.</i> 2013)	2.000	1.997	1.990	1.974	1.964	1.944	1.921	1.895	1.866	1.835	1.802
Current work	2.000	1.997	1.990	1.974	1.964	1.944	1.921	1.895	1.866	1.835	1.802

Table 6 Result validation for vibration of nonlocal uniform circular plate ($\omega a^2 \sqrt{\rho t/D}$)

Boundary condition	η/a	$P = 0$		$P = D/a^2$		$P = 3D/a^2$	
		Current work	(Mohammadi <i>et al.</i> 2013)	Current work	(Mohammadi <i>et al.</i> 2013)	Current work	(Mohammadi <i>et al.</i> 2013)
Simply supported	0.00	4.9351	4.9345	4.3076	4.3076	2.6366	2.6366
	0.05	4.8997	4.8997	4.2709	4.2697	2.5893	2.5830
	0.10	4.7979	4.7979	4.1652	4.1602	2.4504	2.4248
	0.15	4.6415	4.6409	4.0019	3.9910	2.2265	2.1666
	0.20	4.4462	4.4455	3.7963	3.7775	1.9229	1.8081
Clamped	0.00	10.2158	10.2158	9.8704	9.8704	9.1372	9.1372
	0.05	10.1285	10.1283	9.7727	9.7727	9.0158	9.0158
	0.10	9.8788	9.8784	9.4928	9.4928	8.6659	8.6659
	0.15	9.5001	9.4999	9.0660	9.0660	8.1253	8.1253
	0.20	9.0351	9.0348	8.5380	8.5380	7.4420	7.4420

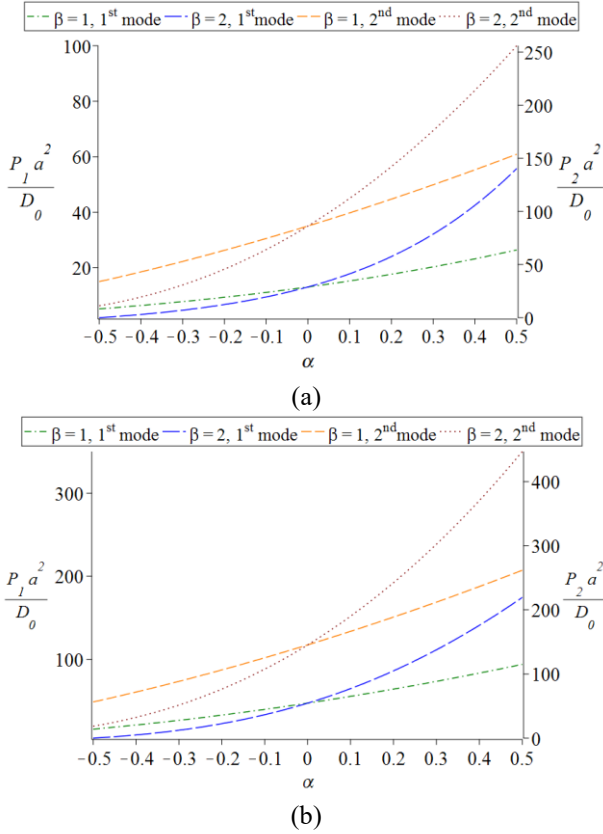


Fig. 4 The effect of taper constant and pattern of thickness variation on two first buckling loads of (a) pinned (b) clamped BDFGSCP

In the case of pinned plate, the results for some values of scale coefficients are slightly different from each other in Table 6. For simplest cases ($\eta = P = 0$), the exact solutions are available. The characteristic equations of vibration for first natural frequency based on classical plate theory for pinned and clamped edges are $I_1(\xi)/I_0(\xi) + J_1(\xi)/J_0(\xi) = 2\xi/(1 - \nu)$ and $I_0(\xi)J_1(\xi) + I_1(\xi)J_0(\xi) = 0$, respectively. The parameters J and I are the Bessel and modified Bessel functions of the first kind. The exact normalized first natural frequency is equal to ξ^2 . In the case of $\eta = P = 0$, the exact normalized first natural frequencies for simply supported and clamped edges are 4.9351 and 10.2158 that are coincide with the current work results.

Figs. 4 and 5 demonstrate dimensionless buckling loads and dimensionless damped natural frequencies of first two modes in pinned and clamped BDFGSCP or RFGSCP for various amounts of α and β . The subscript i in ω_i and P_i denotes mode number. Increasing the values of the parameters α and β yields to increasing damped natural frequencies and buckling loads of two first modes. The effect of taper constant, α , on damped natural frequencies and buckling loads of two first modes for nonlinear thickness variation ($\beta > 1$) is more than linear variation of thickness ($\beta = 1$).

According to Fig. 6, the damped natural frequency of vibration is approached to zero by approaching in-plane compressive radial load to buckling load of corresponding

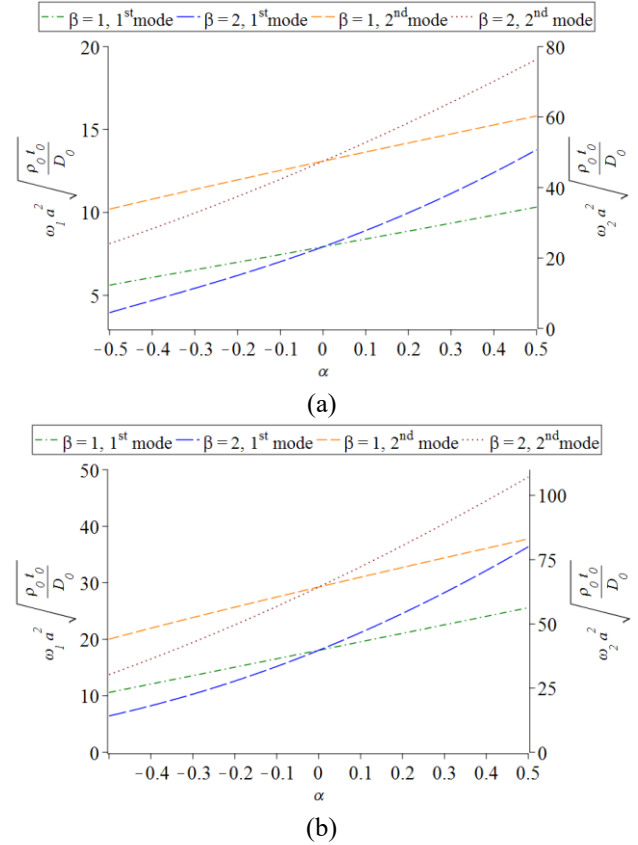


Fig. 5 The effect of taper constant and pattern of thickness variation on two first damped frequencies of (a) pinned and (b) clamped RFGSCP

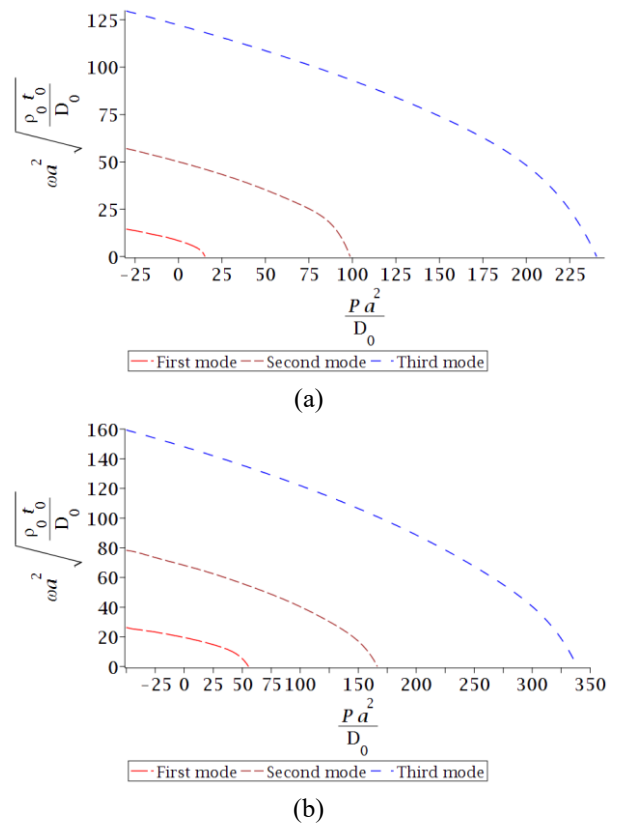


Fig. 6 The effect of in-plane pre-load on first three damped frequencies of (a) pinned and (b) clamped RFGSCP

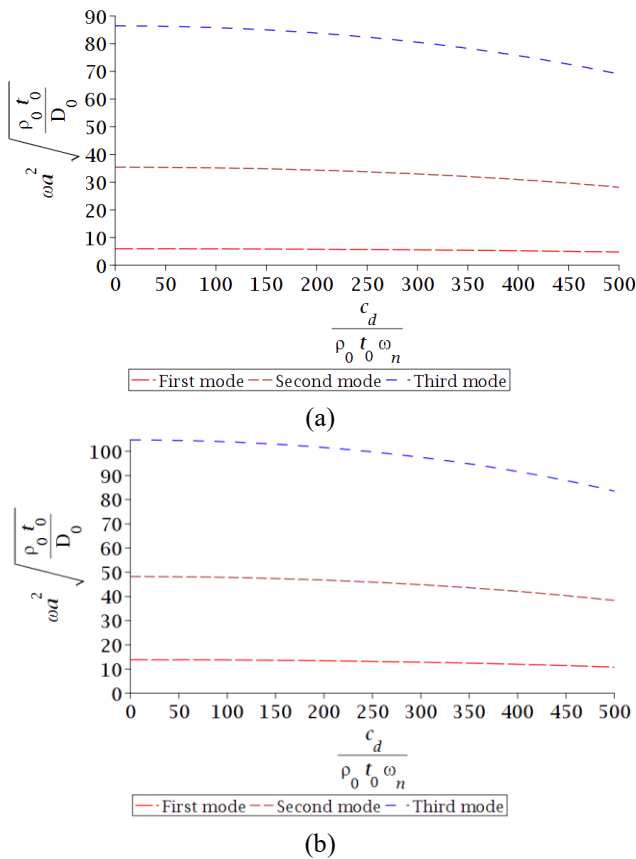


Fig. 7 The effect of viscous medium on dimensionless first three damped frequencies of (a) pinned and (b) clamped BDFGSCP ($R = 3, n_t = 1$)

mode. The compressive radial load decreases damped natural frequency of vibration and the tensile radial load imposed at edge of the plate, increases damped natural frequencies of vibration. The first three damped frequencies of vibration in clamped RFGSCP is more than first three damped frequencies of vibration in pinned RFGSCP.

The effect of viscous medium response on the first three frequencies of vibration of pinned and clamped BDFGSCP is presented in Fig. 7. The transverse material gradation index, n_t , and the dimensionless parameter R are assumed equal to 1 and 3, respectively. The subscript n in parameter ω_n denotes mode number. The dimensionless first three undamped frequencies of BDFGSCP with pinned edge are 5.953, 35.415 and 86.430. By increasing dimensionless ratio of viscous damper coefficient ($c_d/(\rho_0 t_0 \omega_n)$) to 500, the frequencies are decreased to 4.7619, 28.172 and 69.020, respectively. In the case of clamped edge, by increasing dimensionless ratio of viscous damper coefficient to 500, first three normalized frequencies are decreased from 13.835, 48.215 and 104.675 to 10.773, 38.318 and 83.558, respectively.

The effect of material index in radial direction, n_r , and the ratio of top surface to bottom surface properties, R , on undamped natural frequencies of Love-Kirchhoff BDFGSCP with quadratic thickness variation and various boundary conditions is presented in Table 7. Since the parameters n_r and R are mechanical properties of the

Table 7 The normalized fundamental undamped frequency ($\omega a^2 \sqrt{\rho t / D_0}$) of BDFGSCP with quadratic thickness variation ($\beta = 2$) for various material gradation and edge condition

Boundary condition	R n_r	$P = -D_0/a^2$			$P = 0$			$P = D_0/a^2$		
		0.5	1.0	2.0	0.5	1.0	2.0	0.5	1.0	2.0
Pinned	0.5	11.403	10.591	9.529	11.160	10.306	9.182	10.912	10.013	8.821
	1.0	9.875	9.172	8.252	9.665	8.925	7.952	9.450	8.671	7.640
	2.0	8.063	7.489	6.738	7.891	7.287	6.493	7.716	7.080	6.238
Clamped	0.5	25.661	24.649	22.926	25.516	24.476	22.711	25.370	24.301	22.492
	1.0	22.223	21.347	19.855	22.098	21.197	19.668	21.971	21.045	19.479
	2.0	18.145	17.430	16.211	18.043	17.307	16.059	17.939	17.183	15.904

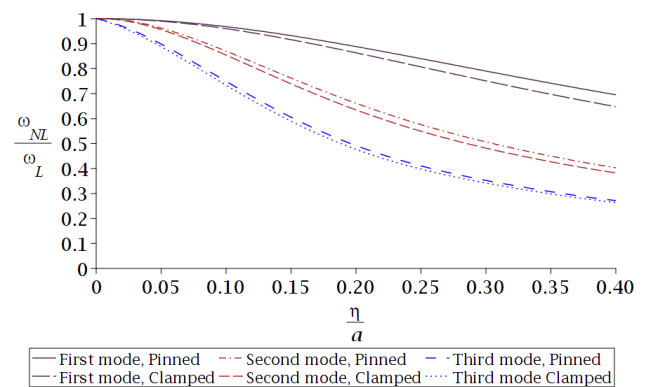


Fig. 8 The effect of scale coefficient on first three damped frequencies of pinned and clamped BDFGSCNPs

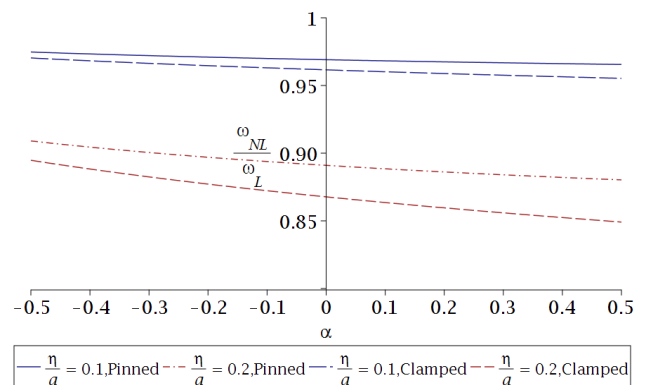


Fig. 9 The effect of taper constant on nonlocal buckling analysis

plate, the response of viscous medium is ignored ($c_d = 0$) to investigate only effects of the mechanical properties and edge conditions of plate on vibrational behavior. According to assumptions in Table 1, the radius to thickness ratio is 25; consequently, the effect of shear deformation can be neglected. In the case of material and mechanical properties which are presented in Tables 1 to 3, increasing material index in radial direction or increasing ratio of top surface to bottom surface properties yields to decreasing normalized frequencies. Fig. 8 presents the effect of scale coefficient on vibrational behavior of BDFGSCP. The ratio of nonlocal damped natural angular frequency of vibration to local

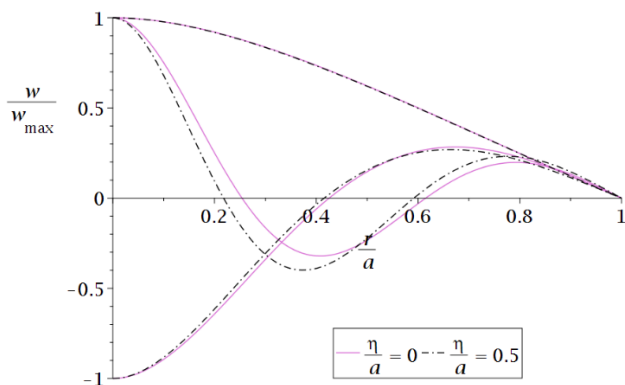


Fig. 10 The effect of scale coefficient on normalized first three vibrational mode shapes

frequency is decreased by increasing scale coefficient. By increasing number of mode, the effect of scale coefficient on decreasing of the ratio of nonlocal structural response to local structural response is increased.

The effect of scale coefficient on size-dependent vibration analysis is presented in Fig. 9. The ratio of nonlocal damped frequency to local damped frequency is decreased by increasing scale coefficient. Increasing taper constant yields to increasing the difference between results of local and nonlocal continuum mechanics. Moreover, in the case of clamped BDFGSCNP the difference between results of local and nonlocal continuum mechanics is more than pinned BDFGSCNP.

The effect of scale coefficient on normalized first three vibrational mode shapes is presented in Fig. 10. The effect of scale coefficient on normalized mode shape is decreased by decreasing mode number.

5. Conclusions

For the first time, nonlocal damped vibration and buckling analysis of arbitrary tapered love-Kirchhoff bidirectional functionally graded solid circular nano-plate (BDFGSCNP) with various boundary conditions at edge of the plate in the presence of viscous medium is presented. A new function with more variables for modeling of two-directional material gradation with more precision than conventional exponential gradation is used to consider variations of mass density and elasticity modulus of bidirectional functionally graded material in cylindrical coordinate. Based on energy method, the neutral equilibrium equation is calculated then the characteristic equations are obtained via fast convergence modified spectral Ritz method by employing a modified basis in terms of orthogonal shifted Chebyshev polynomials of the first kind to eliminate the auxiliary functions. A nontrivial solution is used to calculate undamped natural frequencies of vibration and buckling loads of first modes. The damped and undamped natural frequencies and buckling loads of local BDFGSCP and nonlocal BDFGSCNP are increased by increasing taper constant. Also, the mentioned parameters for plate with clamped boundary condition are more than pinned edge condition. The frequencies of vibration are

decreased by increasing response of viscous medium. The critical load of uniform thin FGSCP with clamped edge is independent from Poisson's ratio. The critical load of simply supported FGSCP is increased by increasing of Poisson's ratio. The damped natural frequency is approached to zero by approaching in-plane compressive radial load to buckling load of corresponding mode. The compressive radial load decreases damped natural frequency of vibration and the tensile radial load increases damped natural frequency of vibration. The effect of taper constant on local and nonlocal damped and undamped natural frequencies and buckling loads, in the case of nonlinear thickness variation is more than linear variation of thickness. The difference between results of local and nonlocal continuum mechanics is increased by increasing scale coefficient and taper constant. In the case of clamped BDFGSCNP the difference between results of local and nonlocal continuum mechanics is more than pinned BDFGSCNP. The effect of scale coefficient on normalized mode shape is decreased by decreasing number of mode. For the simpler cases, an excellent agreement between current work results and outcomes of the previously published results in literature, wherever possible is observed and validity of the current methodology is proved.

References

- Ai, Z.Y., Xu, C.J. and Ren, G.P. (2018), "Vibration of a pre-stressed plate on a transversely isotropic multilayered half-plane due to a moving load", *Appl. Math. Modell.*, **59**, 728-738.
- Arioui, O., Belakhdar, K., Kaci, A. and Tounsi, A. (2018), "Thermal buckling of FGM beams having parabolic thickness variation and temperature dependent materials", *Steel Compos. Struct.*, **27**(6), 777-788.
- Bouderba, B. (2018), "Bending of FGM rectangular plates resting on non-uniform elastic foundations in thermal environment using an accurate theory", *Steel Compos. Struct.*, **27**(3), 311-325.
- Chen, C.S., Liu, F.H. and Chen, W.R. (2017), "Vibration and stability of initially stressed sandwich plates with FGM face sheets in thermal environments", *Steel Compos. Struct.*, **23**(3), 251-261.
- Fallahnejad, M., Bagheri, R. and Noroozi, M. (2018), "Transient analysis of two dissimilar FGM layers with multiple interface cracks", *Steel Compos. Struct.*, **67**(3), 251-261.
- Fang, J., Gu, J. and Wang, H. (2018), "Size-dependent three-dimensional free vibration of rotating functionally graded microbeams based on a modified couple stress theory", *Int. J. Mech. Sci.*, **136**, 188-199.
- Gibigaye, M., Yabi, C.P. and Degan, G. (2018), "Free vibration analysis of dowelled rectangular isotropic thin plate on a modified Vlasov soil type by using discrete singular convolution method", *Appl. Math. Modell.*, **61**, 618-633.
- Gupta, A. and Talha, M. (2015), "Recent development in modeling and analysis of functionally graded materials and structures", *Progr. Aerosp. Sci.*, **79**, 1-14.
- Hadji, L., Amar Meziane, M.A. and Safa, A. (2018), "A new quasi-3D higher shear deformation theory for vibration of functionally graded carbon nanotube-reinforced composite beams resting on elastic", *Struct. Eng. Mech.*, **66**(6), 771-781.
- Heydari, A., Keikha, R., Salkhordeh Haghghi, M. and Hosseinabadi, H. (2018), "Numerical study for vibration response of concrete beams reinforced by nanoparticles", *Struct.*

- Eng. Mech.*, **67**(3), 311-316.
- Heydari, A. (2011), "Buckling of functionally graded beams with rectangular and annular sections subjected to axial compression", *Int. J. Adv. Des. Manufact. Technol.*, **5**(1), 25-31.
- Heydari, A. (2013), "Analytical solutions for buckling of functionally graded circular plates under uniform radial compression using Bessel function", *Int. J. Adv. Des. Manufact. Technol.*, **6**(4), 41-47.
- Heydari, A. (2015), "Spreading of plastic zones in functionally graded spherical tanks subjected to internal pressure and temperature gradient combinations", *Iran. J. Mech. Eng. Trans. ISME*, **16**(2), 5-25.
- Heydari, A. (2017), "A new scheme for buckling analysis of bidirectional functionally graded Euler beam having arbitrary thickness variation rested on Hetenyi elastic foundation", *Modar. Mech. Eng.*, **17**(1), 47-55.
- Heydari, A. and Kazemi, M.T. (2009), "Elasto-plastic analysis of thick-walled FG reservoirs subjected to internal pressure", *Int. J. Adv. Des. Manufact. Technol.*, **3**(1), 11-18.
- Heydari, A. and Kazemi, M.T. (2015), "Thermo-elasto-plastic analysis of functionally graded spherical reservoirs subjected to temperature gradient", *Proceedings of the 10th International Congress on Civil Engineering*, University of Tabriz, Iran.
- Heydari, A. and Shariati, M. (2018), "Buckling analysis of tapered BDFGM nano-beam under variable axial compression resting on elastic medium", *Struct. Eng. Mech.*, **66**(6), 737-748.
- Heydari, A., Jalali, A. and Nemati, A. (2017), "Buckling analysis of circular functionally graded plate under uniform radial compression including shear deformation with linear and quadratic thickness variation on the Pasternak elastic foundation", *Appl. Math. Modell.*, **41**, 494-507.
- Lal, R. and Ahlawat, N. (2017), "Buckling and vibrations of two-directional FGM Mindlin circular plates under hydrostatic peripheral loading", *Mech. Adv. Mater. Struct.*, 1-16.
- Lei, Z.X., Zhang, L.W. and Liew, K.M. (2018), "Modeling large amplitude vibration of matrix cracked hybrid laminated plates containing CNTR-FG layers", *Appl. Math. Modell.*, **55**, 33-48.
- Li, R., Wang, P., Yang, Z., Yang, J. and Tong, L. (2018), "On new analytic free vibration solutions of rectangular thin cantilever plates in the symplectic space", *Appl. Math. Modell.*, **53**, 310-318.
- Li, Y.S., Feng, W.J. and Zhang, C. (2017), "Buckling and vibration of the two-dimensional quasicrystal cylindrical shells under axial compression", *Appl. Math. Modell.*, **50**, 68-91.
- Liew, K.M., He, X.Q. and Kitipornchai, S. (2006), "Predicting nanovibration of multi-layered graphene sheets embedded in an elastic matrix", *Acta Mater.*, **54**(16), 4229-4236.
- Magnucka-Blandzi, E., Wiśniewska-Mleczko, K. and Smyczyński, M.J. (2018), "Buckling of symmetrical circular sandwich plates with variable mechanical properties of the core in the radial direction", *Compos. Struct.*, **204**, 88-94.
- Mohammadi, M., Ghayour, M. and Farajpour, A. (2013), "Free transverse vibration analysis of circular and annular graphene sheets with various boundary conditions using the nonlocal continuum plate model", *Compos. Part B, Eng.*, **45**(1), 32-42.
- Mohammadi, M., Goodarzi, M., Ghayour, M. and Farajpour, A. (2013), "Influence of in-plane pre-load on the vibration frequency of circular graphene sheet via nonlocal continuum theory", *Compos. Part B, Eng.*, **51**, 121-129.
- Naei, M.H., Masoumi, A. and Shamekhi, A. (2007), "Buckling analysis of circular functionally graded material plate having variable thickness under uniform compression by finite-element method", *Proceedings of the Institution of Mechanical Engineers, J. Mech. Eng. Sci.*, **221**(11), 1241-1247.
- Nejad, Z., Rastgoo, A. and Hosseini, M. (2018), "Buckling analysis of FGM Euler-Bernoulli nano-beams with 3D-varying properties based on consistent couple-stress theory", *Steel Compos. Struct.*, **26**(6), 663-672.
- Park, M. and Choi, D.H. (2018), "A two-variable first-order shear deformation theory considering in-plane rotation for bending, buckling and free vibration analyses of isotropic plates", *Appl. Math. Modell.*, **61**, 49-71.
- Ranganathan, S.I., Abed, F.H. and Aldadah, M.G. (2016), "Buckling of slender columns with functionally graded microstructures", *Mech. Adv. Mater. Struct.*, **23**(11), 1360-1367.
- Roshan, L. and Neha, A. (2015), "Buckling and vibrations of two-directional functionally graded circular plates subjected to hydrostatic in-plane force", *J. Vib. Contr.*, **23**(13), 2111-2127.
- Rossit, C.A., Bambill, D.V. and Gilardi, G.J. (2018), "Timoshenko theory effect on the vibration of axially functionally graded cantilever beams carrying concentrated masses", *Struct. Eng. Mech.*, **66**(6), 703-711.
- Sachdeva, C. and Padhee, S.S. (2018), "Functionally graded cylinders, asymptotically exact analytical formulations", *Appl. Math. Modell.*, **54**, 782-802.
- She, G.L., Ren, Y.R., Xiao, W.S. and Liu, H. (2018), "Study on thermal buckling and post-buckling behaviors of FGM tubes resting on elastic foundations", *Struct. Eng. Mech.*, **66**(6), 729-736.
- She, G.L., Ren, Y.R., Yuan, F.G. and Xiao, W.S. (2018), "On vibrations of porous nanotubes", *Int. J. Eng. Sci.*, **125**, 23-35.
- She, G.L., Shu, X. and Ren, Y.R. (2017), "Thermal buckling and postbuckling analysis of piezoelectric FGM beams based on high-order shear deformation theory", *J. Therm. Stress.*, **40**(6), 783-797.
- She, G.L., Yuan, F.G. and Ren, Y.R. (2017), "Nonlinear analysis of bending, thermal buckling and post-buckling for functionally graded tubes by using a refined beam theory", *Compos. Struct.*, **165**, 74-82.
- She, G.L., Yuan, F.G. and Ren, Y.R. (2017), "Research on nonlinear bending behaviors of FGM infinite cylindrical shallow shells resting on elastic foundations in thermal environments", *Compos. Struct.*, **170**, 111-121.
- She, G.L., Yuan, F.G. and Ren, Y.R. (2017), "Thermal buckling and post-buckling analysis of functionally graded beams based on a general higher-order shear deformation theory", *Appl. Math. Modell.*, **47**, 340-357.
- She, G.L., Yuan, F.G. and Ren, Y.R. (2018), "On wave propagation of porous nanotubes", *Int. J. Eng. Sci.*, **130**, 62-74.
- She, G.L., Yuan, F.G., Ren, Y.R. and Xiao, W.S. (2017), "On buckling and postbuckling behavior of nanotubes", *Int. J. Eng. Sci.*, **121**, 130-142.
- Shirmohammadi, F. and Bahrami, S. (2018), "Dynamic response of circular and annular circular plates using spectral element method", *Appl. Math. Modell.*, **53**, 156-166.
- Shojaeefard, M.H., Saeidi Googarchin, H., Ghadiri, M. and Mahinzare, M. (2017), "Micro temperature-dependent FG porous plate, Free vibration and thermal buckling analysis using modified couple stress theory with CPT and FSDT", *Appl. Math. Modell.*, **50**, 633-655.
- Sun, J., Wang, Z., Zhou, Z., Xu, X. and Lim, C.W. (2018), "Surface effects on the buckling behaviors of piezoelectric cylindrical nanoshells using nonlocal continuum model", *Appl. Math. Modell.*, **59**, 341-356.
- Szymczak, C. and Kujawa, M. (2018), "Torsional buckling and post-buckling of columns made of aluminium alloy", *Appl. Math. Modell.*, **60**, 711-720.
- Toghroli, A., Darvishmoghaddam, E., Zandi, Y., Parvan, M., Safa, M., Abdullahi, M.A.M., Heydari, A., Wakil, K., Gebreel, S.A.M. and Khorami, M. (2018), "Evaluation of the parameters affecting the Schmidt rebound hammer reading using ANFIS method", *Comput. Concrete*, **21**(5), 525-530.
- Wang, X., Yang, W.D. and Sheng, G.G. (2014), "Non-linear buckling for the surface rectangular delamination of laminated

- piezoelectric shells”, *Appl. Math. Modell.*, **38**(1), 374-383.
- Xu, Y., Li, Z. and Guo, K. (2018), “Active vibration robust control for FGM beams with piezoelectric layers”, *Struct. Eng. Mech.*, **67**(1), 33-43.
- Yang, Y., Zhang, Y., Chen, W. and Yang, B. (2018), “On asymmetric bending of functionally graded solid circular plates”, *Appl. Math. Mech.*, **39**(6), 767-782.
- Yas, M.H. and Khorramabadi, M.K. (2018), “Mechanical buckling of functionally graded polyethylene/clay nanocomposites columns based on the Engesser-Timoshenko beam theory”, *J. Theoret. Appl. Mech.*, **56**(3), 701-712.
- Yousefzadeh, S., Jafari, A.A. and Mohammadzadeh, A. (2018), “Effect of hydrostatic pressure on vibrating functionally graded circular plate coupled with bounded fluid”, *Appl. Math. Modell.*, **60**, 435-446.

CC